Journal of Geoscience and Environment Protection, 2026, 14(5), 107-122
https://www.scirp.org/journal/gep
ISSN Online: 2327-4344
ISSN Print: 2327-4336

Characterization and Modeling of Fractured Aquifers Using Electrical Resistivity Tomography in Langbabokohou, Bouaké (Central Côte D'ivoire)

Kouamé Gbèlè Hermann Loukou[1,2*], Loukou Nicolas Kouamé[2], Kouao Laurent Kouadio[2,3], Brou Richmond Konan[1,2], Yapo Martial Assi[2]

[1]Unité de Formation et de Recherche des Sciences Géologiques et Minières (UFR-SGM), Département de Géophysique Appliquée, Université de Man, Man, Côte d'Ivoire
[2]Unité de Formation et de Recherche des Sciences de la Terre et des Ressources Minières (UFR-STRM), Laboratoire de Géologie Ressources Minérales et Énergétiques, Équipe de Recherche Géophysique Appliquée, Université Félix Houphouët-Boigny d'Abidjan, Abidjan, Côte d'Ivoire
[3]School of Geosciences and Info-Physics, Central South University of Changsha, Changsha, China
Email: *hermann.loukou@univ-man.edu.ci

How to cite this paper: Loukou, K. G. H., Kouamé, L. N., Kouadio, K. L., Konan, B. R., & Assi, Y. M. (2026). Characterization and Modeling of Fractured Aquifers Using Electrical Resistivity Tomography in Langbabokohou, Bouaké (Central Côte D'ivoire). *Journal of Geoscience and Environment Protection, 14,* 107-122.
https://doi.org/10.4236/gep.2026.145008

Received: February 24, 2026
Accepted: May 25, 2026
Published: May 28, 2026

Abstract

Access to groundwater in crystalline basement regions of West Africa is challenging due to the strong heterogeneity of fractured aquifers and the difficulty in identifying productive zones. In the Bouaké area of central Côte d'Ivoire, high borehole failure rates highlight the need for improved aquifer characterization. This study aims to address this challenge by characterizing and modeling fractured basement aquifers in Langbabokohou using electrical resistivity tomography (ERT) integrated with 3D geoelectrical modeling. Six ERT profiles, oriented N70˚ and spaced 200 m apart, were acquired using the Wenner-Schlumberger array and inverted to obtain true resistivity sections. Resistivity data were analyzed to construct depth-specific maps and a three-dimensional model of the subsurface. Results reveal three main geoelectrical units: a discontinuous, resistive lateritic cover (R1); a conductive weathered layer forming the shallow aquifer (C); and a resistive crystalline basement (R2) overlain by a hydraulically significant fractured horizon. R1 is thin and spatially fragmentary, providing only partial protection to the underlying aquifer. Unit C exhibits low to intermediate resistivity values (25 - 635 Ω·m) and forms a laterally extensive shallow aquifer, while the fractured horizon (635 - 2000 Ω·m) ensures vertical hydraulic connectivity to the deeper basement aquifer. R2 is highly resistive (1723 - 4973 Ω·m) and generally impermeable, except in zones with dense fracturing where groundwater circulation is enhanced. Spatial variability in weathered thickness and fracture density governs aquifer productivity and recharge

efficiency. This study demonstrates that combining ERT with 3D geoelectrical modeling provides a robust framework for understanding basement aquifer architecture, identifying hydraulically active fracture zones, and informing sustainable groundwater management in tropical crystalline terrains.

Keywords

Electrical Resistivity Tomography, Basement Aquifers, 3D Modeling, Groundwater, Côte D'Ivoire

1. Introduction

In crystalline basement regions, sustainable access to groundwater resources is a major challenge, particularly in sub-Saharan Africa, where surface water is often seasonal, highly variable, and intensively exploited for anthropogenic uses. In such contexts, basement aquifers constitute a strategic water resource, although their exploitation remains complex due to pronounced spatial heterogeneity and hydrodynamic behavior governed by weathering processes and fracture networks within crystalline bedrock (Singhal & Gupta, 2010).

In Côte d'Ivoire, and especially in the Bouaké region, the drinking water supply relies mainly on boreholes tapping basement aquifers. However, high failure rates and low yields are frequently reported, reflecting an insufficient understanding of aquifer architecture and the spatial distribution of productive fractured zones (Vouillamoz et al., 2014; MacDonald et al., 2021). Improving hydrogeological exploration strategies, therefore, represents a priority for securing sustainable groundwater resources.

Geophysical methods, particularly Electrical Resistivity Tomography (ERT), have become powerful tools for subsurface imaging in basement environments. These techniques enable discrimination of litho-hydrogeological units, identification of weathered and fractured horizons, and detection of structures controlling groundwater flow (Loke et al., 2013; Binley & Slater, 2020). When combined with three-dimensional modeling approaches, ERT provides an integrated and coherent view of basement aquifer functioning, reducing uncertainties inherent to conventional two-dimensional interpretations (Park et al., 2025; Dewandel et al., 2017).

Although Electrical Resistivity Tomography (ERT) has been widely applied to investigate basement aquifers, many previous studies are limited to 2D interpretations and provide only partial insight into the three-dimensional organization of fracture corridors and their hydraulic role. In particular, there is a lack of integrated studies combining multiple ERT profiles with 3D geoelectrical modeling to explicitly analyze fracture-controlled hydraulic connectivity between shallow weathered aquifers and deeper fractured basement systems.

The research gap addressed in this study lies in the limited understanding of how laterally continuous fracture corridors and weathered-fractured interfaces jointly control groundwater storage and vertical drainage in basement aquifers of

central Côte d'Ivoire. The novelty of this work resides in the integration of six ERT profiles with 3D geoelectrical modeling to characterize the geometry, continuity, and hydraulic significance of fractured horizons at the site scale. This approach allows for improved identification of hydraulically active zones and provides a more reliable framework for groundwater resource assessment and borehole siting in crystalline basement environments.

2. Description of the Langbabokohou Area

The Langbabokohou locality is located in the Bouaké Department, central Côte d'Ivoire. The inhabited area extends between longitudes 313,780 m and 314,310 m and latitudes 839,960 m and 840,530 m (Figure 1). Beyond these limits, the territory extends into agricultural land and secondary vegetation. A 100-ha site located approximately 1 km from the village was selected for geophysical surveys.

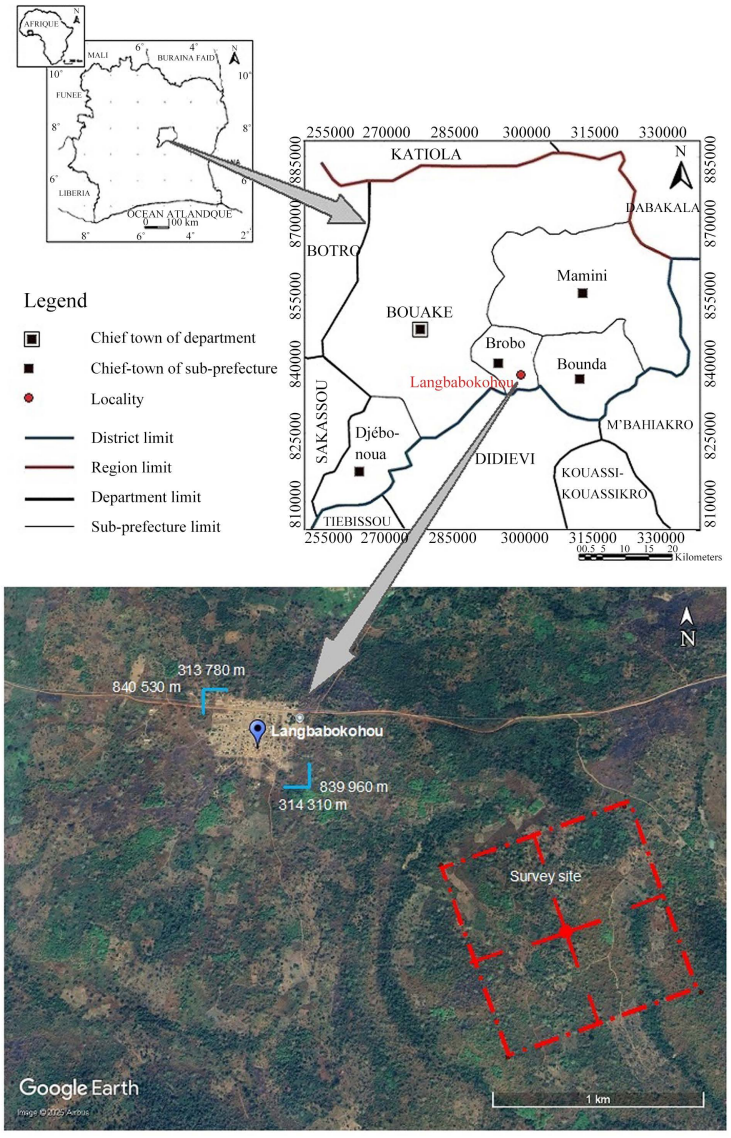

Figure 1. Location of the study area.

All spatial data used in this study are referenced in the Universal Transverse Mercator (UTM) coordinate system and expressed in meters (Easting and Northing). This coordinate system was adopted to ensure accurate spatial positioning of ERT profiles, reliable distance measurements, and consistency with geophysical mapping and field observations.

Three main lithological units are encountered in the area: granite, gneiss, and lateritic cuirass.

At the outcrop scale, the granite is leucocratic and coarse-grained, composed mainly of quartz and feldspar, with minor biotite and muscovite. It occurs as elongated massifs crosscut by quartz veins striking N40˚ (Figure 2).

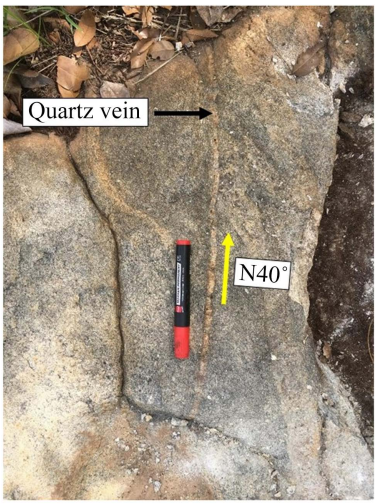

Figure 2. Quartz vein intruding into granite at Langbabokohou.

The gneiss crops out as slab-like exposures covering medium-sized surfaces (10 m × 20 m) and displays a clear mineral segregation (foliation) and stretching lineation. The foliation strikes N30˚, and the unit is affected by an N90˚-oriented fault that shows dextral displacement (Figure 3).

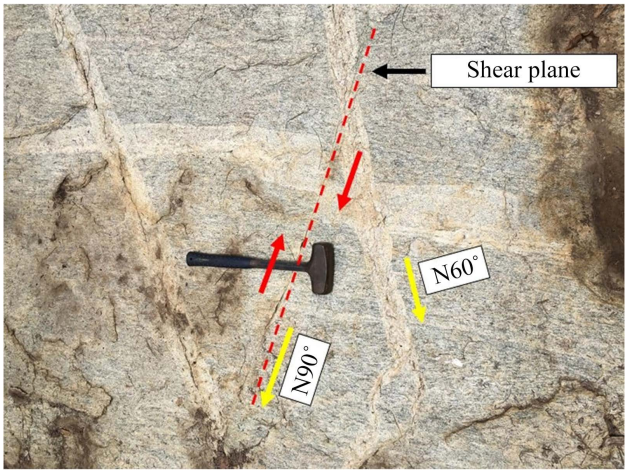

Figure 3. Dextral strike-slip fault in gneiss at Langbabokohou.

Scattered blocks of lateritic cuirass are also observed at the surface (Figure 4). Due to their indurated, compact nature, these materials exhibit high resistivity values comparable to those of granite and gneiss. Unlike the latter, which extends to depth, the cuirass is restricted to the shallow subsurface.

Figure 4. Lateritic duricrust block at Langbabokohou.

3. Methods

3.1. Electrical Resistivity Tomography

ERT surveys were conducted using a Syscal Pro Switch 72 system (Iris Instruments). A total of 36 electrodes spaced 10 m apart were deployed simultaneously along each profile, and automated switching protocols controlled the measurement sequence using the Wenner-Schlumberger array (Figure 5).

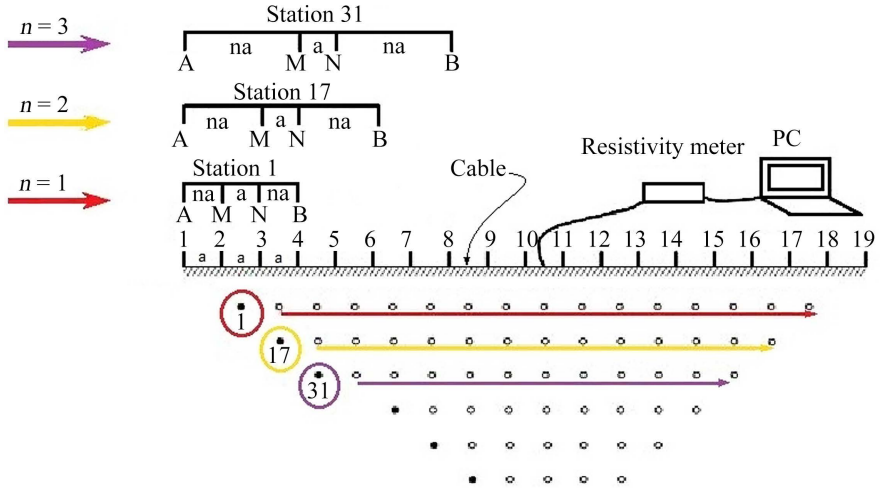

Figure 5. Schematic diagram of the measurement protocol for an electrical resistivity panel using the Wenner-Schlumberger array (modified after Loke et al., 2011).

In this quadrupole configuration, two current electrodes (A and B) inject a direct current of intensity I into the ground, while two potential electrodes (M and N) measure the resulting potential difference ΔV. The apparent resistivity ρ_a is calculated as:

$$\rho_a = \pi n(n+1)a\frac{\Delta V}{I} \quad (1)$$

where ρ_a is the apparent resistivity, n is the spacing factor, a is the distance between potential electrodes M and N, ΔV is the measured potential difference, and I is the injected current.

Six profiles oriented N70˚, each 1070 m long and spaced 200 m apart, were surveyed. A typical acquisition panel covered 320 m, requiring four roll-along sequences to extend each profile. This line orientation was chosen to perpendicularly intersect the site's megafractures, which are oriented N160˚ (Loukou et al., 2022). The survey grid design was guided by established geophysical criteria, aiming to optimize both coverage and resolution. A 200 m line spacing allows mapping of large site sections along the main structural axes, while a 25 m electrode spacing ensures sufficient lateral resolution to detect narrow subvertical fractures. This configuration thus effectively captures fracture-related conductive anomalies while maintaining optimal operational efficiency.

During the survey, all measurements were conducted using consistent acquisition parameters. The duration of the current injection pulse was fixed at 0.5 seconds. A standard deviation threshold of $Q = 0$ was applied. The number of measurement cycles ranged from three to five, with three cycles performed when $Q < 0$ and five cycles when $Q > 0$. The injection voltage during the measurements was maintained at 400 V.

The collected raw data were processed through iterative digital inversion to image the subsurface geological structures. This inversion employed the Gauss-Newton regularization algorithm (Günther, 2004) and was carried out using the Res2DINV software. This program is widely adopted in electrical resistivity imaging due to its effectiveness in inverting complex datasets over heterogeneous layers. The method is based on Equation (2), which minimizes the differences between the observed data and the modeled resistivity at each iteration.

$$\left(S^{\mathrm{T}}D^{\mathrm{T}}DS + \lambda C^{T}C\right)\Delta m_k = S^{\mathrm{T}}D^{\mathrm{T}}D\left(d - f\left(m_k\right)\right) - \lambda C^{\mathrm{T}}C\left(m_k - m_0\right) \quad (2)$$

with:

$$C^{\mathrm{T}}C = \alpha_x C_x^{\mathrm{T}}C_x + \alpha_y C_y^{\mathrm{T}}C_y + \alpha_z C_z^{\mathrm{T}}C_z,$$

where: m_0, reference model; m_k, model at iteration k; S, sensitivity matrix; λ, regularization factor; D, data weighting matrix; C, stress matrix; d, vector of apparent resistivity data containing N values; $f(m_k)$, direct modeling response m at iteration k; α_x, α_y, α_z, anisotropic weights applied in each spatial direction (x, y, z).

This inversion approach is particularly suitable for basement aquifers, where subsurface transitions are generally gradual (Toé, 2004).

3.2. Geoelectrical Modeling

Interpretation of the true resistivity sections allowed the identification of the main geoelectrical units. In each section, points spaced at regular 25-m intervals were selected to define litho-logs, representing the vertical succession of units with their respective top and bottom depths. This approach generated a set of spatially distributed "virtual boreholes".

It is important to note that no borehole logs, pumping data, or water-level observations were available for this site. Therefore, the fractured horizon and hydraulic activity presented in this study are based solely on geoelectrical data and 3D modeling and should be considered as interpretations rather than confirmed hydrogeological conditions.

These data were imported into Surpac software to construct a continuous three-dimensional model. For each geoelectrical unit, corresponding blocks were correlated across all sections. Spatial interpolation between litho-log points was performed using the inverse distance weighting (IDW) method:

$$\rho_i = \frac{\sum_{j=1}^{n} w_{ij}\rho_j}{\sum_{j=1}^{n} w_{ij}}, \quad w_{ij} = \frac{1}{d_{ij}^{p}} \tag{3}$$

where ρ_i is the estimated resistivity of block i, ρ_j are neighboring values, d_{ij} is the distance between points, and p is the weighting exponent. This method enabled reconstruction of the volumetric geometry of each unit and the development of a coherent 3D subsurface model.

4. Results

4.1. True Resistivity Sections

Interpretation of the true resistivity sections reveals three main geoelectrical units (Figure 6):

- A resistive unit R1 composed of scattered blocks;
- A conductive horizon C;
- A resistive unit R2.

The three geoelectric units (resistant surface cover, conductive alterite or horizon, and highly resistant sound bedrock) are clearly defined in each section. The resistivity ranges and lithological correlations of these geoelectrical units are summarized in Table 1.

The resistive unit R1 exhibits resistivity values typically ranging from 850 to 1723 Ω·m, with locally higher values reaching approximately 3000 Ω·m. Based on field observations and geoelectrical interpretation, R1 is interpreted as a superficial lateritic cover composed mainly of scattered cuirass blocks.

Spatially, R1 is discontinuous and fragmentary. It is clearly identified along profiles L00, L200 N, L400 N, and L600 N, where it occurs as localized lenses or blocks. Conversely, it is nearly absent along profiles L800 N and L1000 N, indicating enhanced erosion processes toward the northern part of the site. This heterogeneous distribution reflects the progressive dismantling of the superficial cover during landscape evolution.

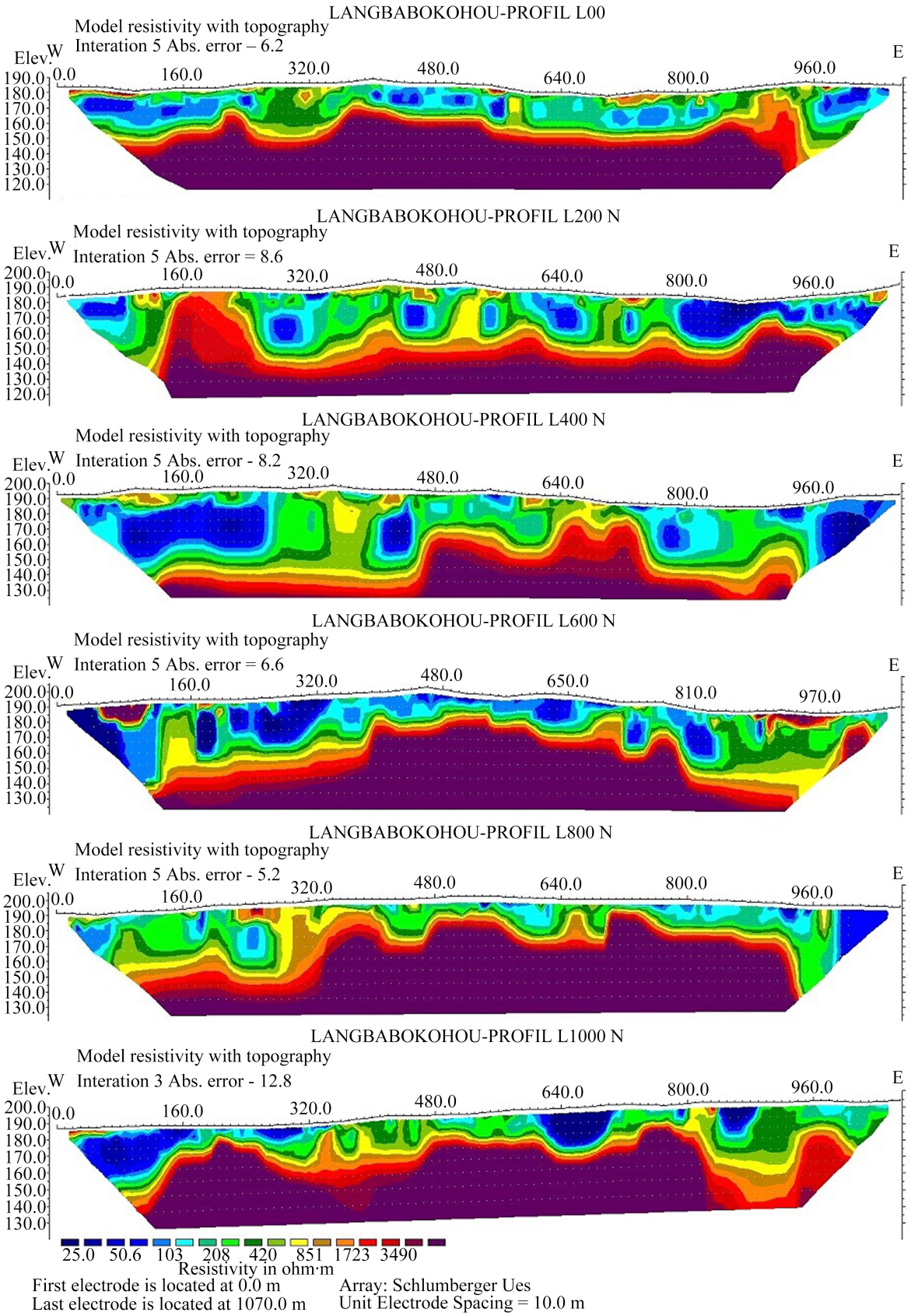

Figure 6. True resistivity sections of profiles L00, L200 N, L400 N, L600 N, L800 N, and L1000 N.

Table 1. Resistivity ranges and lithological correlations of the surveyed formations.

Layer	Geoelectrical unit		Resistivity range [Ω·m]	Lithology	Hydrogeological conditions
Top	R1		850 - 1723	lateritic duricrust	dry and impermeable
Middle	C		25 - 635	alterite	moist and permeable
Base	R2	upper part	635 - 2000	cracked horizon	fractured and permeable
		lower part	1723 - 4973	sound crystalline basement	compact and impermeable

The thickness of R1 is generally very limited, rarely exceeding 5 m. This reduced thickness, combined with its lateral discontinuity, strongly limits its volumetric influence within the hydrogeological system.

From a hydrogeological perspective, R1 primarily serves as a protective cover over the underlying conductive unit C, which corresponds to the weathered aquifer. When present, R1 limits direct infiltration of surface water and reduces the risk of contamination. Conversely, its absence or limited development increases exposure of unit C, thereby increasing the shallow aquifer's vulnerability to anthropogenic pollution. Therefore, R1 does not constitute an aquifer itself but represents the residual upper part of the weathering profile, whose main function is aquifer protection.

Beneath R1 lies the conductive unit C, which is widely developed and represents the most laterally extensive and hydrogeologically significant unit.

Unit C is characterized by low resistivity values, mainly ranging from 25 to 155 Ω·m, reflecting the presence of electrically conductive materials. Intermediate resistivity levels (155 - 635 Ω·m) are frequently observed within this unit, indicating lateral and vertical variations related to the degree of weathering, porosity, and water saturation. These resistivity contrasts reflect marked internal heterogeneity.

Lithologically, unit C corresponds to weathered materials derived from basement alteration, composed of clayey-sandy, lateritic, or sandy-clayey formations. Its thickness varies significantly across the site, ranging from a few meters (~5 m) in eroded zones to 35 - 40 m in areas where weathering and/or saturation is more developed. This substantial thickness provides Unit C with significant groundwater storage capacity.

Spatially, unit C is continuous at the site scale, although locally interrupted by higher-resistivity zones corresponding to slightly weathered basement. These internal discontinuities do not compromise the overall coherence of the conductive unit, which remains dominant across all investigated profiles.

Hydrogeologically, unit C represents the main shallow aquifer of the Langbabokohou site. Its variable porosity and permeability favor infiltration and storage of meteoric water, making it a seasonal capacitive reservoir, particularly active during the rainy season. This aquifer is commonly exploited by traditional wells and also contributes to the recharge of deeper boreholes.

At depth lies the resistive unit R2. The transition between unit C and the resistive basement R2 is not abrupt but occurs through an intermediate resistivity horizon (635 - 2000 Ω·m), interpreted as a fractured basement horizon. This horizon plays a key role in vertical groundwater drainage, ensuring hydraulic connectivity between the shallow aquifer and the deeper fractured basement aquifer.

Unit R2 is characterized by high resistivity values, generally ranging from 1723 to 4973 Ω·m, typical of slightly weathered to fresh crystalline basement with low primary porosity and low electrical conductivity. Relative resistivity homogeneity observed along some profiles indicates massive, weakly fractured bedrock, whereas local variations reflect structural discontinuities.

The depth to the top of unit R2 varies significantly across the site, reflecting an irregular basement morphology. It may be shallow (~5 m) in some areas (profiles L00, L200 N, and L800 N) and reach 30 - 60 m in the central or western sectors (profiles L400 N and L600 N). This variability reflects differential weathering intensity of the basement.

Along most profiles, unit R2 exhibits an intermediate resistivity zone at its top, interpreted as a fractured horizon. This zone corresponds to increased fracturing and microfracturing resulting from tectonic stresses and mechanical weathering, providing a gradual transition between conductive weathered materials and fresh basement.

Hydrogeologically, unit R2 represents the deep basement aquifer, whose productivity depends primarily on fracture density and connectivity. Where the basement is massive and weakly fractured, its contribution to groundwater storage and flow is limited. Conversely, major faults and densely fractured zones, particularly along profiles L1000 N (faults F1 and F2) and the eastern end of profile L600 N, confer high hydrogeologic potential by enhancing groundwater circulation and storage.

Thus, unit R2 forms the structural and hydrodynamic framework of the Langbabokohou aquifer system. Its interaction with the fractured horizon and the conductive weathered unit C controls overall system functioning by ensuring both vertical drainage of infiltrated water and long-term storage within fractured basement zones.

4.2. Resistivity Maps by Level

Based on the apparent resistivity pseudo-sections, iso-resistivity maps for levels 2, 7, and 12 were generated (**Figure 7**). These levels correspond to pseudo-depths of 10 m, 25 m, and 45 m, respectively, in a Wenner-Schlumberger configuration. Overlaying these maps by depth enables assessment of both vertical and lateral subsurface structure.

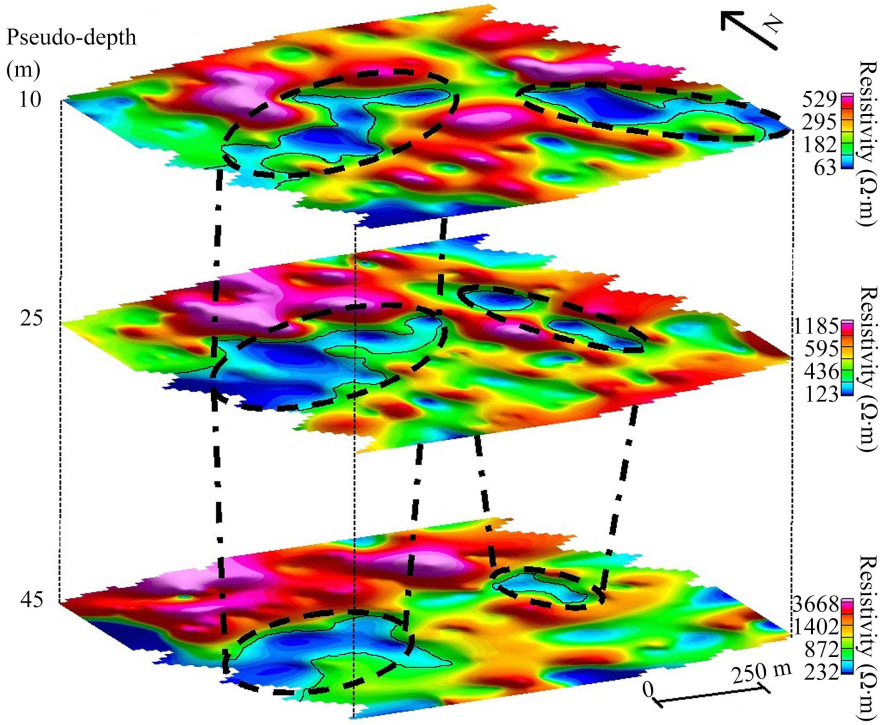

Figure 7. Overlaid resistivity maps for levels 2, 7, and 12.

At the 10 m pseudo-depth, the resistivity distribution, ranging from 60 to 550 Ω·m, exhibits strong heterogeneity, with a predominance of conductive zones interpreted as weathered formations and shallow terrains locally saturated with water.

At the 25 m pseudo-depth, resistivity contrasts become more pronounced (100 - 1200 Ω·m), reflecting a gradual transition from weathered formations to more resistive layers. Conductive zones persist but tend to narrow and align along preferential NNW-SSE directions, suggesting structural control.

At the 45 m pseudo-depth, resistivities generally increase (200 - 3700 Ω·m), indicating the presence of basement. Resistive domains dominate, while conductive zones, more restricted and well-defined, correspond to deep fractured zones of the basement. These fractures also follow the NNW-SSE orientation observed at 25 m pseudo-depth.

A correlative (vertical) analysis of levels 2, 7, and 12 highlights the rooting of major conductive anomalies, indicated by dashed lines, and reveals fracture structures extending through all investigated levels. The vertical continuity of these fractures indicates hydraulic activity, linking the weathered layer to the fractured basement and enhancing both groundwater flow and the hydrogeological potential of the basement aquifer.

4.3. Conceptual Model of the Aquifer

The three-dimensional conceptual model obtained by integrating resistivity sections highlights a well-organized vertical and lateral structure. The volumetric dis-

tribution of resistivity contrasts enables the clear identification of four major geoelectric units, whose geometry and connectivity govern the system's hydrogeological functioning (Figure 8).

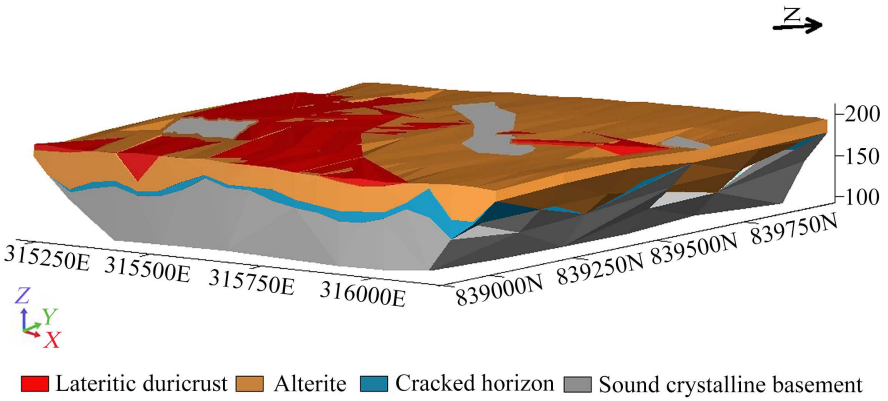

Figure 8. 3D conceptual model of the Langbabokohou aquifers.

The lateritic duricrust, characterized by high resistivities, appears as blocky and locally thick at the top of the model. Its lateral discontinuity reflects differential preservation of the duricrust, strongly controlled by surface morphology and erosion processes. Its indurated, low-porosity character suggests a primarily protective role against underlying weathering while locally acting as a partial barrier to direct infiltration of meteoric water. The spatial distribution of this unit indicates that its hydrogeological influence is secondary and strongly dependent on the degree of superficial fracturing.

Beneath the duricrust, the weathered horizon represents the dominant unit in terms of lateral extent. Its variable thickness reflects differential substrate weathering, controlled by lithology, the density of inherited structural discontinuities, and basement topography. This horizon plays a key role as a temporary storage zone and a vertical conduit for infiltrated water to deeper levels.

The fractured horizon constitutes the hydrogeological core of the system. It develops preferentially at the weathered layer-intact basement interface, with an undulating geometry and lateral continuity over much of the model. The relatively low resistivities of this unit indicate a significant increase in secondary porosity, attributable to an open, water-saturated fracture network. The vertical continuity of this horizon, locally connected to the overlying weathered layers, suggests strong hydraulic connectivity and efficient groundwater transfer. Zones where the fractured horizon thickens coincide with depressions in the basement top, indicating pronounced structural control and localized fracture concentration.

The intact crystalline basement, characterized by high resistivities, underlies the model and corresponds to granitic rock, based on field petrographic observations. It is sparsely fractured and poorly permeable. Its irregular geometry reveals substrate relief controlled by deep structures, likely inherited from the regional tectonic history. Basement uplift zones are associated with thinning of the weathered

and fractured horizons, reflecting unfavorable hydrogeological conditions. Conversely, basement subsidence areas favor the development of a thicker weathered cover and a more interconnected fractured horizon, thereby constituting preferential zones for groundwater circulation and accumulation.

Overall, the 3D conceptual model demonstrates spatial coherence between basement structuring and the distribution of conductive units. The lateral and vertical continuity of conductive zones suggests the presence of major fracture corridors that act as preferential hydraulic conduits. This architecture aligns with conceptual models of basement aquifers, in which borehole productivity is primarily controlled by the thickness and connectivity of the fractured horizon and by the presence of a sufficiently developed weathered cover to ensure recharge.

5. Discussion

5.1. Weathering Profile and Structural Control

True resistivity sections, level-specific maps, and the 3D conceptual model reveal a characteristic vertical and lateral organization of the subsurface typical of crystalline basement aquifers in humid tropical environments. The succession of resistive-conductive units (R1-C-R2), together with their geometry and connectivity, reflects a polyphase weathering profile controlled by substrate lithology, weathering intensity, and inherited tectonics.

The superficial lateritic duricrust (R1), though locally well-expressed (>850 Ω·m), is spatially discontinuous and thin, indicating advanced dismantling due to differential erosion and current morphodynamics. This observation aligns with West African studies showing that duricrust preservation strongly depends on topography and surface stability (Beauvais & Chardon, 2013; Dewandel et al., 2017). Its near absence in northern profiles exposes the weathered layer directly, reinforcing lateral heterogeneity.

Beneath, the conductive horizon C dominates both laterally and in thickness (locally 35 - 40 m). Measured resistivities (25 - 155 Ω·m) and higher intermediate values indicate pronounced internal heterogeneity, reflecting variations in weathering degree, material texture, and water content. This structure corresponds to progressive weathering models in crystalline basement, where weathered layers evolve vertically from a conductive clay-sandy horizon to coarser, more resistive levels (Wyns et al., 2004; Lachassagne et al., 2021).

Level-specific resistivity maps further highlight lateral structuring. At 10 m, resistivity heterogeneity reflects variable surface formations and locally saturated zones. At 25 m, conductive lineaments aligned NNW-SSE suggest structural control, likely due to inherited fractures or shear zones. At 45 m, these trends persist within the basement, where conductive anomalies mark deep fractures. The directional coherence and vertical continuity of these anomalies indicate deep structures traversing the weathering profile, confirming that basement topography and fracture distribution govern the organization of geoelectric units (Singhal & Gupta, 2010; Vouillamoz et al., 2014).

5.2. Hydro-Dynamic Functioning of the Aquifer System

The geoelectric architecture at Langbabokohou reflects typical basement-aquifer functioning, controlled by interactions among the weathered cover, the fractured horizon, and the intact basement. The conductive horizon C functions as a capacitive shallow aquifer, temporarily storing meteoric water and gradually transferring it to deeper levels. Its lateral extent and local thickness make it a strategic reservoir, particularly for shallow wells.

Discontinuous lateritic duricrust limits direct recharge locally. Where absent or thinned, the shallow aquifer is exposed, increasing vulnerability to anthropogenic contamination. This partial protection is typical of tropical weathered environments, where duricrust provides localized rather than continuous shielding (Taylor & Howard, 2000; MacDonald et al., 2021).

The transition from conductive weathered layers to resistive basement R2, represented by an intermediate resistivity horizon (635 - 2000 Ω·m), is key to hydrodynamic functioning. This fractured horizon, extensively developed at the weathered layer-basement interface, features enhanced secondary porosity from fracturing and mechanical weathering. Its lateral continuity and vertical connection with overlying layers enable efficient drainage toward the deep aquifer. Thickened zones, often coinciding with basement depressions, are hydrogeologically favorable, whereas basement uplifts, with thinned weathered and fractured layers, are less favorable. These patterns are consistent with recent studies of West African basement aquifers (Dewandel et al., 2017; Courtois et al., 2020).

The intact crystalline basement (R2), although generally resistive and poorly permeable, becomes hydrogeologically significant locally where affected by faults or dense fractures, as observed in profiles L600 N and L1000 N. The vertical continuity of conductive anomalies from weathered layers to fractured basement confirms hydraulic activity and links shallow and deep aquifers. These fracture corridors serve as preferential drains, enhancing both flow and long-term storage.

Overall, the 3D conceptual model highlights a hierarchical aquifer system in which functioning relies on the complementarity of a capacitive shallow aquifer and a fractured deep aquifer. Borehole productivity is primarily controlled by the thickness and connectivity of the fractured horizon and by the presence of a sufficiently developed weathered cover to ensure recharge. This organization aligns with current conceptual models of West African basement aquifers and supports the relevance of integrated geoelectrical approaches for sustainable groundwater management.

6. Conclusion

The study conducted at Langbabokohou highlighted the geoelectric structuring and hydrodynamic functioning of a crystalline basement aquifer under humid tropical conditions. Integration of true resistivity sections, level-specific resistivity maps, and three-dimensional geoelectric modeling led to the identification of three major units: a discontinuous superficial lateritic duricrust, a conductive weathered hori-

zon forming the shallow aquifer, and a resistive crystalline basement overlain by a hydraulically significant fractured horizon.

Results indicate that the shallow aquifer, although capacitive and extensive, exhibits strong lateral variability and increased vulnerability in areas lacking protective duricrust. The fractured horizon, located at the weathered layer-basement interface, constitutes the key component of the system, ensuring hydraulic connectivity between shallow and deep reservoirs. The vertical continuity of conductive anomalies highlights hydraulically active fracture corridors, preferentially oriented NNW-SSE, which govern groundwater flow and accumulation.

The 3D conceptual model emphasizes that potential borehole productivity is primarily controlled by the thickness and connectivity of the fractured horizon, as well as by the sufficient development of the weathered cover. These findings confirm the value of electrical tomography as a decision-support tool for hydrogeological exploration in basement terrains and provide a solid scientific basis for more rational and sustainable groundwater management in the Bouaké region and, more broadly, in West African crystalline basement contexts.

Practically, productive boreholes should target areas where the conductive weathered layer is thick (>30 m) and connected to the fractured horizon along these fracture corridors. Areas with shallow basements and thin or discontinuous weathered cover should be avoided. Protection of recharge zones with limited duricrust is essential to preserve water quality and ensure sustainable aquifer management.

Conflicts of Interest

The authors declare no conflicts of interest regarding the publication of this paper.

References

Beauvais, A., & Chardon, D. (2013). Modes, Tempo, and Spatial Variability of Cenozoic Cratonic Denudation: The West African Example. *Geochemistry, Geophysics, Geosystems, 14,* 1590-1608. https://doi.org/10.1002/ggge.20093

Binley, A., & Slater, L. (2020). *Resistivity and Induced Polarization: Theory and Applications to the Near-Surface Earth.* Cambridge University Press. https://doi.org/10.1017/9781108685955

Courtois, N., Lachassagne, P., Wyns, R., Blanchin, R., Bougaïré, F. D., & Somé, S. (2020). Large-Scale Mapping of Hard-Rock Aquifer Properties Applied to Burkina Faso. *Groundwater, 48,* 269-283. https://doi.org/10.1111/j.1745-6584.2009.00620.x

Dewandel, B., Lachassagne, P., Wyns, R., Maréchal, J. C., & Krishnamurthy, N. S. (2017). A Generalized 3D Geological and Hydrogeological Conceptual Model of Granite Aquifers Controlled by Single or Multiphase Weathering. *Journal of Hydrology, 330,* 260-284. https://doi.org/10.1016/j.jhydrol.2006.03.026

Günther, T. (2004). *Inversion Methods and Resolution Analysis for the 2D/3D Reconstruction of Resistivity Structures from DC Measurements.* Ph.D. Thesis, University of Mining and Technology.

Lachassagne, P., Wyns, R., Dewandel, B., & Courtois, N. (2021). Basement Aquifers: Characterization and Modeling. *Journal of Hydrology, 594,* Article ID: 125641.

Loke, M. H., Chambers, J. E., & Kuras, O. (2011). Instrumentation, Electrical Resistivity. In H. K. Gupta (Ed.), *Encyclopedia of Earth Sciences Series* (599-604). Springer. https://doi.org/10.1007/978-90-481-8702-7_191

Loke, M. H., Chambers, J. E., Rucker, D. F., Kuras, O., & Wilkinson, P. B. (2013). Recent Developments in the Direct-Current Geoelectrical Imaging Method. *Journal of Applied Geophysics, 95,* 135-156. https://doi.org/10.1016/j.jappgeo.2013.02.017

Loukou, K. G. H., Kouamé, N., & Sombo, B. C. (2022). Contribution of Aeromagnetism to the Lithostructural Identification of the Aquifer System of Bouaké Department (Central Ivory Coast). *IOSR Journal of Applied Geology and Geophysics (IOSR-JAGG), 10,* 1-11.

MacDonald, A. M., Bonsor, H. C., Dochartaigh, B. É. Ó., & Taylor, R. G. (2021). Quantitative Maps of Groundwater Resources in Africa. *Environmental Research Letters, 7,* Article ID: 024009. https://doi.org/10.1088/1748-9326/7/2/024009

Park, S., Cheon, Y., Kim, T., & Choi, J. (2025). Applicability of Electrical Resistivity Surveys for Tracing and Characterizing Active Faults: A Case Study in the Northern Gongju Fault Zone, Korea. *Episodes, 48,* 295-305. https://doi.org/10.18814/epiiugs/2024/024028

Singhal, B. B. S., & Gupta, R. P. (2010). *Applied Hydrogeology of Fractured Rocks* (2nd ed.). Springer.

Taylor, R., & Howard, K. (2000). A Tectono-Geomorphic Model of the Hydrogeology of Deeply Weathered Crystalline Rock: Evidence from Uganda. *Hydrogeology Journal, 8,* 279-294. https://doi.org/10.1007/s100400000069

Toé G. (2004). *Apport de nouvelles techniques géophysiques à la connaissance des aquifères de socle—Tomographie électrique, Electromagnétisme fréquentiel, Résonance Magnétique Protonique: Application au Burkina Faso* (p. 272). Thèse de Doctorat, Université Paris.

Vouillamoz, J. M., Lawson, F. M. A., Yalo, N., Descloitres, M., & Vouillamoz, P. (2014). The Use of Magnetic Resonance Sounding for Quantifying Specific Yield and Transmissivity in Hard Rock Aquifers: The Example of Benin. *Journal of Applied Geophysics, 107,* 16-24. https://doi.org/10.1016/j.jappgeo.2014.05.012

Wyns, R., Baltassat, J. M., Lachassagne, P., Legtchenko, A., & Vairon, J. (2004). Application of Proton Magnetic Resonance Soundings to Groundwater Reserve Mapping in Weathered Basement Rocks (Brittany, France). *Bulletin de la Société Géologique de France, 175,* 21-34. https://doi.org/10.2113/175.1.21